Experimental study on gas permeability characteristics of Biochar-Amended Loess

Wenqi Zhao [1], Xi-An Li [2,*]

Chang'an University, Xi'an, Shaanxi, 710064, China

Abstract: Gas permeability is an important parameter to characterize the permeability and structure of soil. In this paper, the air permeability test of Mâlain loess with different water content and biochar content is carried out by using the improved air permeability meter, and the pore characteristics of the sample are Quantitative analysis from the microscopic level. The test results show that the gas permeability coefficient of soil increases first and then decreases with the increase of water content, and reaches the maximum at 16%. With the increase of biochar content, the gas permeability coefficient of soil decreases first and then increases, and there is an optimal content of biochar in the modified loess. The probability division index of pore area increases first and then decreases, and the average pore area decreases first and then increases the frequency of pore orientation is the largest in the range of 0 ° to 10 °, the overall performance is anisotropic, and there is a dominant direction in the local area. The roundness of pores is concentrated in the range of 0.3 to 0.4, and the shape of pores is mainly irregular.

1 Introduction

Loess is a kind of natural loose sediments with large pores and rich in carbonate, which was transported and deposited by wind during the Quaternary period, with high compressibility, collapsibility, and low strength and other adverse engineering characteristics. It is widely distributed in the Midwestern Sectional Figure Skating Championships of our country, with an area of 640,000 km^2, accounting for about 6.6% of the total land area of China. It is the main battlefield of "Western development" and "Belt and Road development" in China. The permeability of soil includes water permeability and air permeability. At present, scholars at home and abroad have studied the characteristics of water permeability more abundantly, but the research on the characteristics of air permeability is relatively few, therefore, it is of great significance to carry out continuous experimental study on gas permeability characteristics. Firstly, the gas permeability coefficient can also characterize the permeability characteristics of soil, and the test process is simpler and shorter. Secondly, there is a good double logarithmic linear relationship between the gas permeability coefficient and the permeability coefficient [1], the permeability coefficient obtained by the correlation is more accurate because the gas permeability test can avoid the strong water sensitivity of loess; in addition, the gas permeability coefficient plays an important role in tunnel construction, pollution removal and landslide control.

Biochar is a new type of modified material produced by high-temperature pyrolysis of plant-based biomass in an oxygen-free or anoxic environment, it has the characteristics of low density, high specific surface area, high porosity and high chemical stability [2], in recent years, it has been widely concerned by scholars at home and abroad and is considered to be a promising overlying soil landfill and replacement material. Wan et al [3]. studied the effect of biochar content and type on the gas permeability of compacted silt, and established a prediction model for the permeability coefficient of biochar-modified soil. Li Mingyu et al. [4] obtained a linear relationship between the gas permeability coefficient and the particle size of biochar by studying the gas permeability characteristics of biochar modified clay. Z. Sun et al. [5] found that biochar can change the pore structure parameters of sand, increase the total porosity, and then increase the gas permeability coefficient of soil by adding biochar to sand. Zhan et al. [6] studied the influence of sample size and water content on the air permeability of loess, and found that high water content hinders the air permeability of loess when the sample size is large.

From the above research, we can conclude that the change of water content and biochar content will have a great influence on the permeability of soil. In this paper, the improved air permeability instrument was used to conduct air permeability tests on Mâlain loess with different water contents (12%, 14%, 16%, 18%, 20%) and biochar contents (0%, 5%, 10%, 15%, 20%), and the variation curves of air permeability coefficient were obtained. The pore characteristics of the specimens were Quantitative analysis at the microscopic level using a

[1]Email: 3032116734@qq.com
[2*]Email: dclixa@chd.edu.cn

Phenom and a PCAS (pore (particle) and fracture image recognition and analysis system), the change of gas permeability coefficient under different conditions was compared. This paper provides suitable design conditions and parameters for the modification of loess by biochar as landfill or replacement material.

2 Test device and method

2.1 Material and sample preparation

The loess used in the experiment is Mâlain loess (Q3) of the Quaternary Upper Pleistocene in Jingyang district, Xi'an. It is an eolian loess with more vertical pores than horizontal pores and obvious anisotropy, the main composition is mixed clay minerals such as illite and Montmorillonite, and the composition is mainly silt particles. The sample depth is 5 m. Using rice straw as raw material, biochar was obtained by pyrolysis, cooling, filtration, grinding and sieving at 500 °C for 30-40 minutes in an oxygen-limited environment.

According to the standard of soil test method and the standard test method for chemical analysis of charcoal, the relevant physical index parameters of the test material were obtained, the basic physical parameters of loess and biochar are shown in Table 1.

Table 1. Basic physical parameters of experimental loess and biochar

Loess of Malan							Biochar		
liquid limit /%	plastic limit /%	plastic index	max dry density /(g·cm^{-3})	optimum moisture content / %	Specific gravity	PH	specific area /(m^2·g^{-1})	specific gravity	ash content /%
30.84	16.55	14.29	1.68	16.95	2.7	9.8	1042	1.98	20.3

After natural air-drying, the undisturbed soil sample was crushed by a rubber hammer, passed through a 2 mm sieve, and then dried in an oven for 8 h at 105 °C to obtain a dry soil with a moisture content of nearly 0%. The biochar was mixed with dry soil using a blowing method, stirred and shaken, and then stored under seal for 48 h. the mixed sample was mixed with deionized water by spray method, any large aggregates produced in the mixing process were crushed by chopsticks and prepared into a sample with a certain moisture content. The sample was sealed in a cool place for 48 hours. The mixed soil sample was compacted three times by static layered compaction method, cylindrical specimens with a dry density of 1.50 g/cm3, a diameter of 8 cm, and a height of 8 cm were prepared, need to layer parts for shaving treatment, in the wall coated with a layer of Vaseline.

2.2 Gas permeation device

The air permeability test device is based on the ZC-2015 air permeability meter and the SL-12 permeameter. The instrument is Modular design and consists of a water-gas consolidation permeability tester module, a water permeability coefficient module and a gas permeability coefficient module (as shown in Figure 1). The principle of the test is to pump the air inside the instrument through a vacuum pump, form a certain negative pressure inside the instrument, form a pressure difference with the external atmospheric pressure, and enter the instrument as the air passes through the sample, thus the pressure difference between the instrument and the outside is reduced, and the change rate of mercury scale in different time is obtained, and then the gas permeability coefficient in the process of variable pressure difference is obtained. The gas permeability measurement range of the test device is 10^{-10}~10^{-16} m^2.

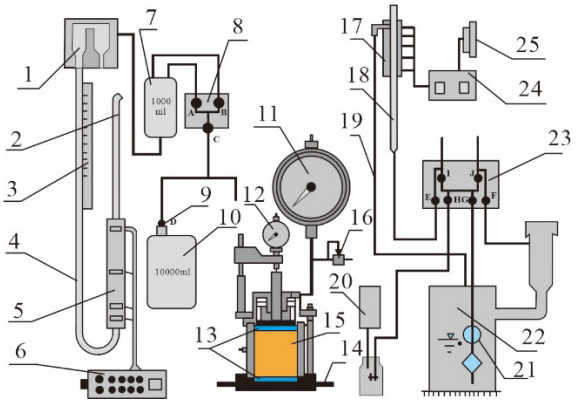

1. Buffer chamber; 2. Mercury import 3. Ruler 4. U-bank tube 5. Infrared photoelectric module 6. Intelligent measurement and control system 7.1000ml air chamber 8. Valve group (A, B, C)9. Valve D10.10000ml air chamber 11. Precision pressure gauge 12. Percent table 13. Upper and lower permeable stones 14. Pipe joints 15. Specimen cylinder 16. Pressure relief valve 17. Miniature vacuum pumps 18. Pressure measuring tube 19. Return water pipe 20. Vacuum system 21. Water pumps 22. Water tank 23. Valve assembly (E, F, G, H, I, J)24. Controller 25. Display screen

Figure 1. Improved water-air consolidation and penetration tester

The gas medium used in the experiment is air, and the air flow in the soil samples belongs to slow seepage. The calculation of soil gas permeability satisfies the gas Fick law and Darcy law. Based on the influence of pressure difference on experimental results, the calculation method for gas permeability coefficient refers to the cylindrical flow model calculation method proposed by Hong Bo [7]. The calculation formula is as follows:

$$K_a = \frac{ELV}{AP_{atm}t}\ln\frac{y_0}{y} \quad (1)$$

In this equation, K_a is the gas permeability coefficient

(m^2), y_0 is the scale (m) corresponding to the mercury column at the initial pressure, y is the height (m) of the Mercury column at any time t, E is the air viscosity coefficient (Pa·s) , L is the effective permeation path (m) , A is the area of gas permeability (m^2) , V is the volume of the closed system (m^3) , and P_{atm} is the atmosphere area (Pa).

2.3 Microscopic Test

In order to avoid the influence of boundary effect, the interior of each group of samples was selected for cutting sample preparation. The sample was a cylindrical sample with a bottom diameter of 1 cm × a height of 1 cm. The sample was frozen in liquid nitrogen for 30 min, and then it was placed in a freeze dryer, epoxy, acetone, ethylenediamine and dibutyl phthalate were mixed in a volume ratio of 100:200:7:2 (Hao Zhitao [8]) and stirred until a transparent reagent was formed The reagent is injected into the soil sample by the dropping method, and then the vacuum pump is used for vacuum treatment to enhance the injection effect of the reagent in filling the internal pores of the soil. After sealing for one month, after the sample is hardened, special instruments are used for cutting, polishing and polishing, Phenom Scanning electron microscope are used to obtain 800X magnified SEM images, and PCAS is used for post-processing and data acquisition. Figure 5 is the SEM image, binary image and vector image of pore characteristics. Table 2 is the mathematical statistics of pore size, quantity, area and perimeter after quantitative analysis.

In order to describe the distribution characteristics of pore area, the concept of area cumulative distribution function is used in this paper, which reflects the density of pore areas within a specific region and describes the change in the number of pores as the pore area increases. The expression for this function is cited from Liu Chun [9]:

$$F(S) = aS^{-b} \tag{2}$$

$$S = S_0 2^{n-1} \tag{3}$$

$$b > 1,\ a = \frac{1-b}{(2^{n(1-b)}-1)S_0^{1-b}}$$

$$b = 1,\ a = \frac{1}{nln2} \tag{4}$$

In the formula, F(S) is the probability density of the corresponding area of pores, b is the probability distribution index (the greater the value of b, the less the number of large-area pores), the value of a is related to b, and S is the area of a particular area, n is the number of ranges (n = 1,2,3...,), S_0 is the minimum pore area.

The pore orientation distribution frequency Fi (α) is commonly used to indicate the directivity and arrangement characteristics of pores. A higher pore orientation distribution frequency indicates a greater number of pores within a specific directional interval. The expressions are:

$$F_i(\alpha) = \frac{n_i}{N} \times 100\% \tag{5}$$

In the equation: (n_i) represents the number of pores within the i-th orientation; N is the total number of pores; α represents the orientation angle of pores arranged within the 0° to 180° range, where this study selects α=10° as the orientation angle interval and divides 180° into 18 intervals.

The form factor (*ff*) is an important parameter for describing pore morphology. It is related to the pore area (S) and perimeter (C), and ranges from 0 to 1. In this study, the form factor is used to describe the circularity of the pores. A form factor closer to 1 indicates that the pore shape is closer to circular, while a lower value reflects irregularity. The expression for the form factor is:

$$ff = \frac{4\pi S}{C^2} \tag{6}$$

3 Results

Figure 2 shows the relationship between the gas permeability coefficient and the compacted moisture content of Biochar-Amended Loess at different biochar contents, with a dry density of 1.50g/cm^3. From the graph, it can be observed that the gas permeability coefficient of BAL generally exhibits an increasing trend followed by a decreasing trend as the compacted moisture content increases. When the compacted moisture content is less than 16%, the gas permeability coefficient gradually increases with the moisture content, and the rate of change becomes faster. However, when the moisture content exceeds 16%, the gas permeability coefficient shows a negative correlation with the moisture content. Furthermore, the effect of compacted moisture content on the gas permeability coefficient is related to the biochar content. When the biochar content is less than 5% or greater than 15%, the compacted moisture content has a minor impact on the gas permeability coefficient. Conversely, when the biochar content is between 5% and 15%, the impact of the compacted moisture content on the gas permeability coefficient increases with higher biochar content.

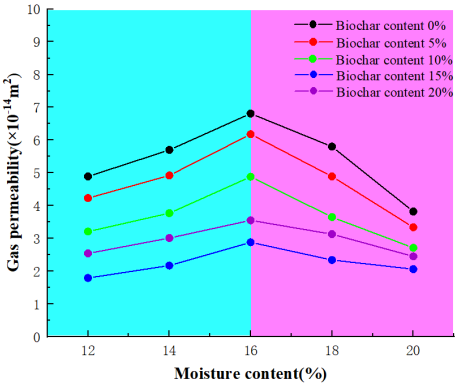

Figure 2. Relationship between gas permeability coefficient and compaction water content in Biochar-Amended Loess

Figure 3 shows the cumulative particle size distribution curves for soil samples with different biochar contents. It can be observed from Figure 4 that when the biochar content is less than 15%, the proportion of small and medium particles in the mixed soil gradually decreases, while the proportion of large particles increases. When the biochar content exceeds 15%, the proportion of small particles remains almost unchanged,

the proportion of large particles gradually decreases, and the proportion of medium particles gradually increases.

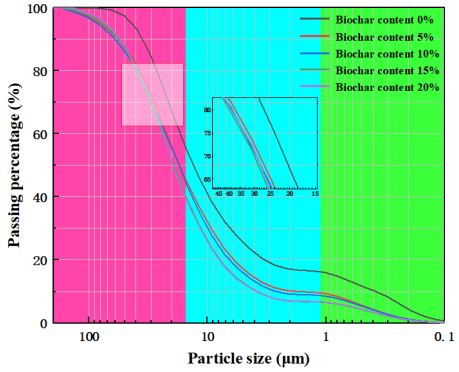

Figure 3. Particle size distribution cumulative curves of mixed soils with different biochar contents

From Figure 5, it can be observed that as the specific area pore volume increases, the probability distribution function curve of pore area gradually decreases, and the decreasing trend shows an initial increase followed by a decrease as the biochar content increases, i.e., the b value initially increases and then decreases. Figure 6 shows the distribution frequency of large, medium and small pore areas in five groups of different areas. As can be seen from the figure, with the increase of biochar content, there is a noticeable change in pore density within the area, and overall, the number of large pores decreases first and then increases, while the number of small pores gradually increases. The analysis indicates that when the biochar content is low, the filling effect dominates, and with increasing biochar content, the filling effect improves, leading to a gradual reduction in the number of large pores. When the biochar content exceeds 15%, the filling effect no longer dominates, and a carbon skeleton structure forms between the biochar particles, resulting in an increase in the number of large pores.

Table 2. Basic parameters of micro-pores of loess with different biochar contents

Biochar content/%	Region number	Average region area /pixel	Average perimeter /pixel	Average length /pixel	Average width /pixel
0	614	292.47	90.45	26.78	15.19
5	750	247.96	85.06	25.01	14.26
10	1062	226.88	82.02	23.86	14.08
15	752	168.98	72.26	22.07	12.33
20	1042	208.41	77.71	23.37	13.72

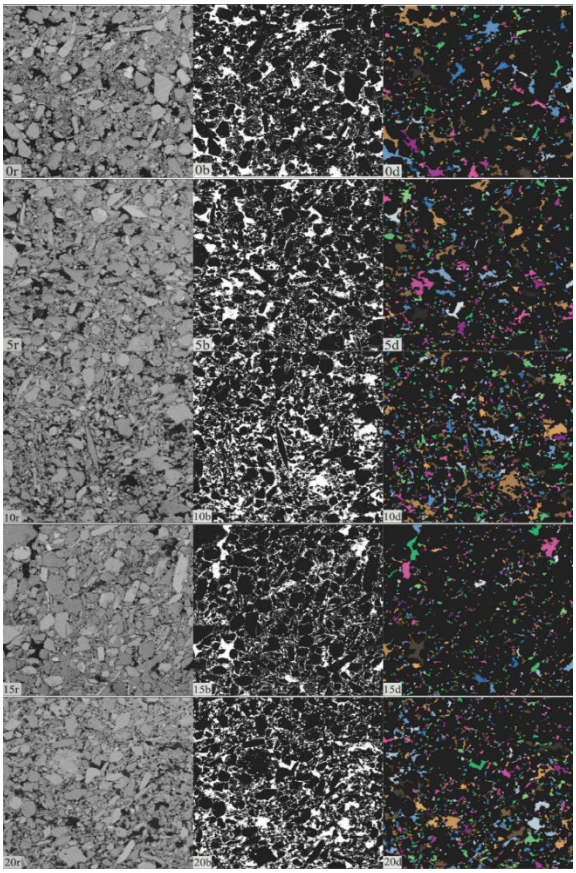

Figure 4. SEM raw images, binary images and pore distribution image of the five samples (The designation code on the bottom left was designed to differentiate the images. The first number indicates the content of biochar; "r", "b" and "d" represent the original image, the binary image and pore distribution image respectively

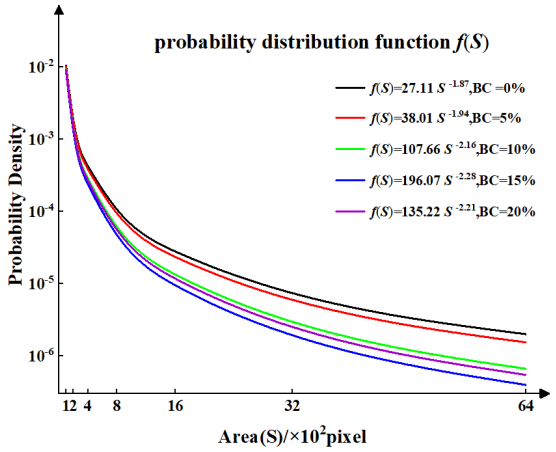

Figure 5. Approximate power function curves of pore area probability density distribution in samples with different biochar contents

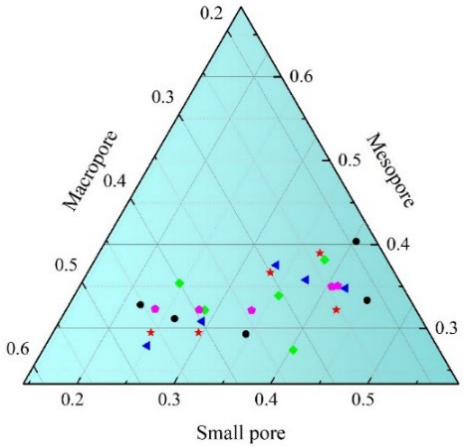

Figure 6. Pore area frequency three-phase diagram (S=6400 pixel)

Assuming a mirror distribution of pore orientation frequency between the 0°~180° and 180°~360° ranges, a rose diagram of pore orientation frequency for different biochar contents is plotted based on the proportion of pores in each directional interval, as shown in Figure 7.

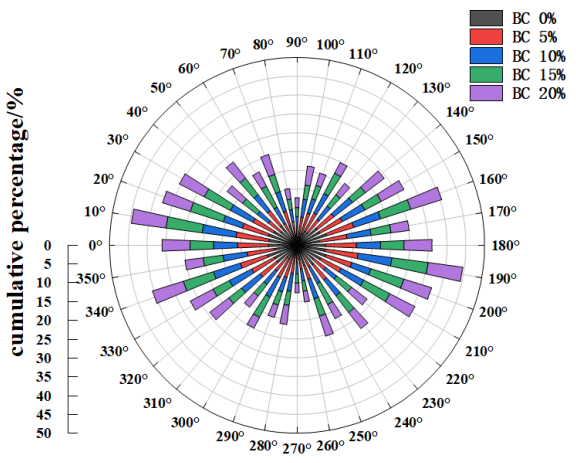

Figure 7. Rose diagram of pore orientation frequency in Biochar-Amended Loess (BC: biochar content)

From Figure 7, it can be observed that with the increase in biochar content, there is a minor fluctuation in the pore orientation frequency, showing a pattern of decrease or increase in specific intervals. Looking at the cumulative percentage content, pore orientation frequency is distributed in all intervals, with relatively higher distribution in the 0°~10° and 150°~160° intervals, lower distribution in the 80°~90° interval, and moderate distribution in the remaining directional angle intervals. This indicates that with the increase of biochar content, there is a predominant direction in the pore orientation frequency. The reason for this could be attributed to the porous sheet-like structure of biochar particles and the face-to-face stacking contact mode between the biochar particles and the loess particles. As the biochar content increases, it becomes difficult for the particle orientation to change, resulting in minimal changes in pore orientation. Overall, this leads to a relatively stable behavior. Additionally, the increase in biochar content weakens the inter-particle bonding, causing minor deviation in pore orientation under the action of external forces and internal water and gas molecule migration, leading to increased directionality and the presence of predominant directions in localized areas.

According to the formula (6), the variation of the pore roundness of the Biochar-Amend Loess with different contents is shown in Figure 8.

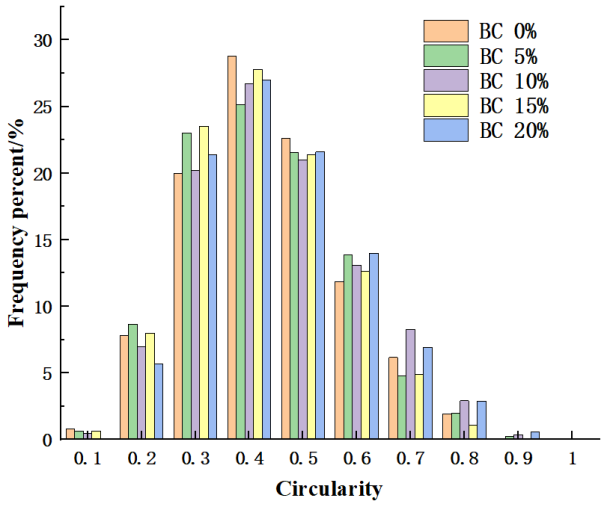

Figure 8. Pore morphology of Biochar-Amended Loess (BC: biochar content)

It can be seen from Figure 8 that the circularity of pores changes obviously. Specifically, circularity demonstrates an overall decrease in fluctuation in the 0~0.2 and 0.4~0.5 intervals, an increase in fluctuation in the 0.2~0.3 and 0.5~0.8 intervals, and initially decreasing and then increasing fluctuation in the 0.3~0.4 interval. As for content distribution, pore circularity is primarily concentrated between 0.3~0.4, followed by 0.2~0.3 and 0.4~0.5. This indicates that the shapes of the pores in the sample are mostly irregular. Furthermore, the circularity is not significantly influenced by the biochar content, suggesting that the variation trend of pore circularity is minimally affected by the biochar content.

4 Discussion

The above results reveal the basic patterns of the influence of different moisture content, biochar content, and particle size on the gas permeability of loess. In this context, further research is needed to explore and understand the reasons for the poor gas permeability in loess modified with biochar.

4.1 Gas permeability model and parameters

The primary factors influencing the gas permeability of soil are pore characteristics, including porosity, pore connectivity, tortuosity, as well as pore quantity, area, and size. At present, the commonly used model for predicting soil air infiltration is a power function based on soil-air volume content, considering pore connectivity and tortuosity as the main influencing factors. (Moldrup et al. [10]). For example, Equation (7):

$$K_a = \alpha V_g^{\beta} \tag{7}$$

Where Ka is the gas permeability coefficient (m2); α is the pore connectivity parameter; Vg is the gas volume content; and β is the water resistance factor. Equations (8) and (9) describe the relationship between gas volume content, saturation (S_w), and porosity(n), as well as the relationship between factors affecting soil saturation.

$$V_g = (1 - S_w)n \tag{8}$$

$$S_w = \frac{w\rho_d G_s}{(G_s - \rho_d)\rho_w} \tag{9}$$

Figure 9 shows the relationship curves between saturation and moisture content, as well as biochar content under constant dry density conditions. It can be observed from the figure that both saturation and moisture content, as well as biochar content, exhibit a positive linear correlation. Additionally, the influence of biochar content on saturation change is far greater than that of moisture content.

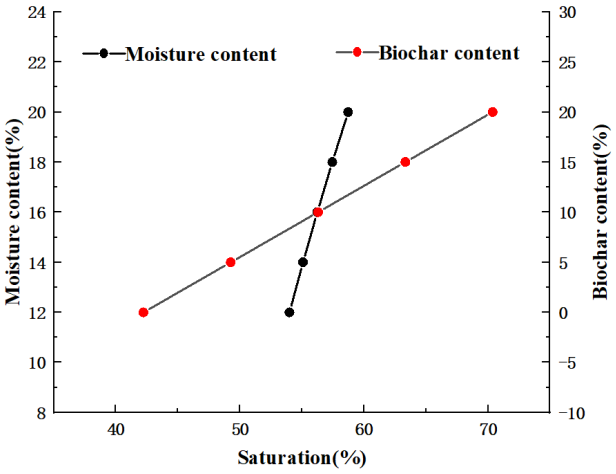

Figure 9. Relationship between saturation, moisture content and biochar content

Substituting equation (8) into equation (7) yields equation (10):

$$K_a = \alpha(1 - S_w)^{\beta} n^{\beta} \tag{10}$$

To eliminate the influence of porosity on permeability, a normalization correction is applied to the permeability coefficient following the Kozeny-Carmen model, yielding: [insert equation].

$$\frac{K_a}{\frac{n^3}{(1-n)^2}} = \alpha(1 - S_w)^{\beta} \tag{11}$$

Based on equation (11), the relationship between the corrected gas permeability coefficient and saturation is obtained (as shown in Figure 10). By fitting the power function curve, predictive values for pore connectivity and water resistance factor at different biochar contents can be derived. Linear fitting of the predicted values for α and β at different biochar contents yields the relationship curve between porosity and α, β values (as shown in Figure 11).

As shown in Figure 11, both the pore connectivity parameter α and the water resistance factor β increase with increasing porosity. This phenomenon indicates that when the dry density is constant and moisture content remains unchanged, the reduction in porosity caused by an increase in biochar content leads to a more pronounced water resistance effect, poorer pore connectivity, and a gradual decrease in the permeability coefficient.

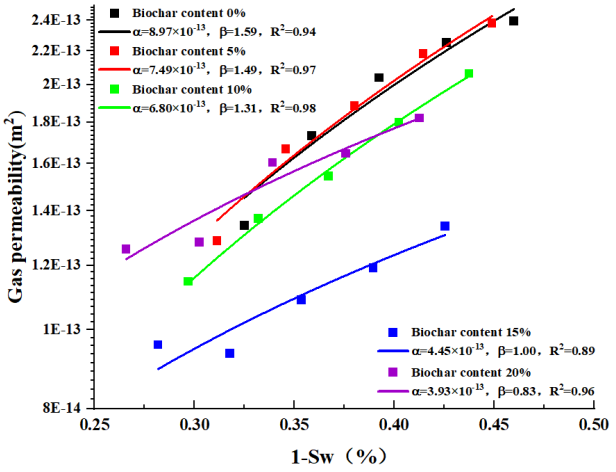

Figure 10. Relationship between normalized gas permeability and saturation

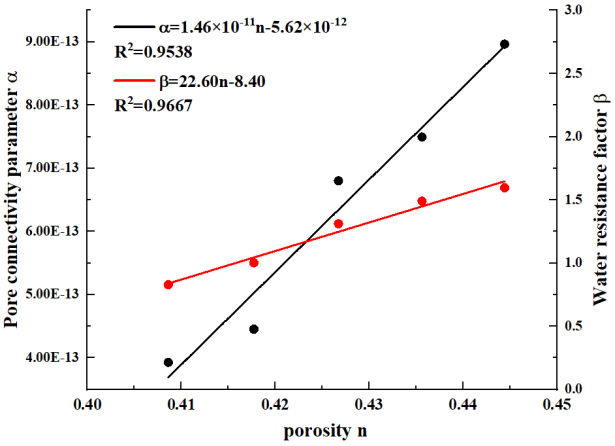

Figure 11. Relationship between porosity (n) and connectivity coefficient (α), water resistance factor (β)

4.2 Effect of water content in compaction on gas permeability

The passage describes the investigation of the impact of moisture content on the gas permeability of BAL by varying the compacted water content. The experimental results indicate that moisture content significantly affects the gas permeability of biochar-modified loess. The analysis suggests several reasons for this observation: ① At lower moisture content, internal pore water within the soil occupies only a small fraction of the gas flow pathway volume. Consequently, the gas flow path length is relatively longer. As the moisture content increases, the proportion of pore water occupying the gas flow pathway to some extent increases. This gradual filling of pore water from terminal branching pores to main interconnected pores reduces the tortuosity of the gas flow pathways, enhances pore connectivity to some degree, and decreases the gas penetration path, thereby increasing the gas permeability of the soil (Tuli et al. [11]). ② At lower moisture content, water molecules adhere between soil particles and aggregates in the form of capillary and adsorbed water. With increasing moisture content, a smooth water film gradually forms on their surfaces, reducing the frictional resistance between structural units to some extent and consequently enhancing the gas permeability of the specimen. ③ With increasing moisture content, certain clay minerals and soluble salts in loess gradually dissolve and dissociate, forming ionized compounds. This process softens the original internal structure of the soil, reducing its hindrance to gas flow. However, this promotion effect due to increased moisture content is not always effective. When the moisture content exceeds the plastic limit of the soil, pore water no longer exists in forms such as capillary curvature liquid surfaces but reaches a flowing state in the soil. This flowing water will act to block larger pore channels in the soil, thus decreasing the gas permeability.

4.3 Effect of biochar on gas permeability of loess

The above results demonstrate that when the biochar content is 5%, 10%, 15%, and 20% respectively, the gas permeability coefficient of compacted BAL decreases by 1.1, 1.4, 2.4, and 1.92 times compared to the gas permeability coefficient of natural loess (as shown in Figure 2). Therefore, the optimum mixing ratio of biochar is 15%, which is consistent with the research findings of Li Mingyu et al.

The influence of biochar content on the gas permeability of BAL is manifested in several aspects: ① When the biochar content is low, an increase in biochar content leads to a gradual increase in the total porosity within the soil, resulting in an increased number of gas flow pathways. And as the biochar content increases, its filling effect becomes more pronounced, leading to a gradual reduction in the number of large pores and a weakening of gas permeability. (Figure 12) ② The surface of biochar is rich in hydrophilic functional groups (-COOH, -OH, -CO) (Suliman et al. [12]). Upon interaction with water, the thickness of the bound water film on the surface and internal pore walls of biochar particles significantly increases (Grag et al. [13]). This reduces the proportion of free water molecules and the effective diameter of the pore channels, increasing the resistance to gas flow through water and thus reducing gas permeability. ③ When the biochar content reaches a certain level, its hydrophilicity gradually diminishes and may even exhibit hydrophobic properties (Dugan et al. [14]), thereby reducing the water stability of aggregates. Therefore, the content of large particles and aggregates within the mixed soil does not continually increase. ④ At higher biochar contents, the impact of the increased total porosity due to the multi-porous structure of biochar and the formation of a carbon framework with relatively large pores between biochar particles becomes predominant, leading to an increase in gas permeability.

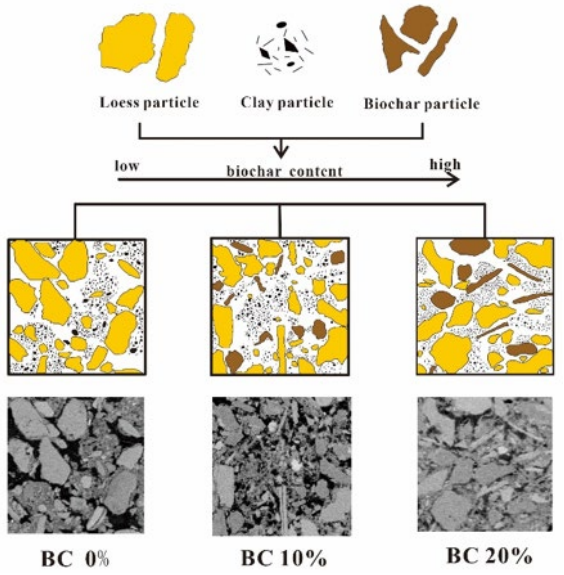

Figure 12. Conceptual model of Biochar-Amended Loess (BC: biochar content)

5 Conclusion

By using the improved soil water-gas consolidation permeation meter, the gas permeation of mixed soil samples with different biochar content, particle size and compaction water content was tested, and combined with the quantitative analysis results of pore characteristics after scanning electron microscope and PCAS image processing, the following conclusions were drawn:

(1) With increasing compaction moisture content, the gas permeability coefficient initially increases and then decreases, reaching a maximum value near the optimal moisture content. The magnitude of the increase and decrease trends gradually diminishes as the compaction moisture content moves away from the vicinity of the optimal moisture content

(2) The gas permeability rate of the mixed soil samples shows a trend of decreasing initially and then increasing with increasing biochar content. This indicates the existence of an optimal mixing ratio that minimizes the gas permeability coefficient. When the biochar content exceeds this optimal ratio, the gas permeability coefficient

exhibits a rebound-type growth.

(3) As the biochar content increases, the probability distribution index of pore area exhibits a trend of initial increase followed by decrease, with a gradual reduction in the number of large pores and an initial decrease followed by an increase in average pore area. The orientation frequency of pores is highest within the 0°to 10° range, indicating the overall performance is anisotropy, and the local dominant direction exists. The pore circularity is concentrated in the 0.3 to 0.4 range, the shape of pores is mainly irregular.

References

1. Zhao Min, He Hui. (2005) Experimental study on water-gas permeability in unsaturated loess [J]. Journal of Xi'an University of Science and Technology, 25(3): 292-295
2. Lehmann J. Bio-energy in the black [J]. Frontiers in Ecology and he Environment, 2007, 5(7): 381–387.
3. Wan Y, Dong Z, Xingxing He Rui qi Liu Yangyang Cai Lei Liu Linbo Qin Qiang Xue. Effect of biochar on permeability of compacted soil and its microscopic mechanism[J]. Canadian Geotechnical Journal, 2022, 59(12). DOI:10.1139/cgj-2021-0586.
4. Li Mingyu, Sun W J, et al. (2022) Study on gas permeation characteristics of biochar modified landfill cover soil [J]. Chinese Journal of Rock Mechanics and Engineering 41(S2): 3543-3550. 2022.0041.
5. Sun Z, Moldrup P and Elsgaard L et al. (2013) Direct and indirect short-term effects of biochar on physical characteristics of an arable sandy loam[J]. Soil Science, 178(9): 465–473.
6. Zhan T L T , Yang Y B , Chen R ,et al. Influence of cl od size and water content on gas permeability of a co mpacted loess 1[J].Canadian Geotechnical Journal, 2 014, 51(12):1468-1474.DOI:10.1139/cgj-2014-0126.
7. Hong B. (2020) Experimental study on water-air heat conduction characteristics and heat and humidity transport law of loess [D]. Chang 'an University
8. Xue Q. A New Method for Evaluating the Homogen eity and Structure of Remolded Loess Samples with the Air Permeability Coefficient[J]. Applied Sciences, 2022, 12.DOI:10.3390/app12199412.
9. Liu Chun (2011) Quantification and characterization of microporosity by image processing, geometric measurement and statistical methods: Application on SEM images of clay materials
10. Moldrup, P., Yoshikawa, S. and Olesen, T. et al. (2003). Air permeability in undisturbed volcanic ash soils: predictive model test and soil structure fingerprints. Soil Science Society of America Journal 67, 32–40.
11. Tuli, A. and Hopmans, J.W. (2004). Effect of degree of fluid saturation on transport coefficients in disturbed soils. European Journal of Soil Science, 55(1):147–164.
12. Suliman W, Harsh J B and Abu-lail N I, et al.(2017) The role of biochar porosity and surface functionality in augmenting hydrologic properties of a sandy soil [J]. Science of the Total Environment ,574:139-147.
13. Garg, A., Huang, H. and Cai, W et al. (2021) Influence of soil density on gas permeability and water retention in soils amended with in-house produced biochar. Journal of Rock Mechanics and Geotechnical Engineering, 13(3): 593–602.
14. Dugan E, Verhoef A and Robinson S et al.(2010) Biochar from sawdust, maize stover and charcoal: Impact on water holding capacities (WHC) of three soils form Ghana[C].19th World Congress of Soil Science, Soil Solutions for a Changing World. Brisbane, Australia: [s. n.]